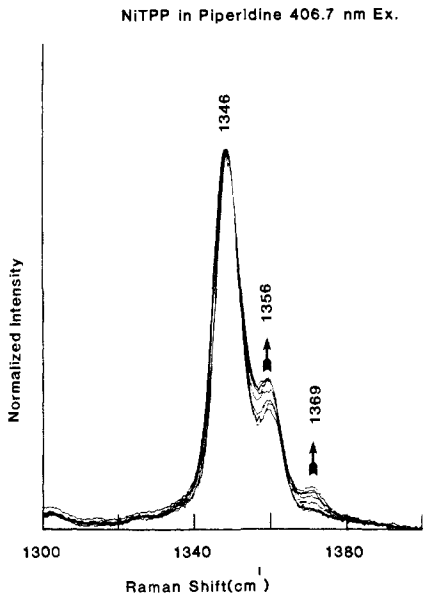

Figure 3. ν_4 Raman peaks for a stationary sample of NiTPP, 0.5 mM in piperidine, with 406.7-nm excitation. Arrows indicate the increasing relative intensities of the 1356- and 1369-cm^{-1} peaks with increasing laser power (5, 15, 25, 50, 75, 100, 125, and 150 mW): 5-cm^{-1} slit width; 1-s time constant; 0.5 cm^{-1}/s scan rate. The spectra were scaled to the 1346-cm^{-1} peak.

The spectra in Figure 1 show a progressive augmentation of the 1369-cm^{-1} band and diminution of the 1346-cm^{-1} band with increasing incident laser power levels. The intensity ratio is plotted against laser power in Figure 2, where it is seen to increase monotonically from a starting value of 0.54 to a limiting value of $\sim$1.6. When the sample was spun through the laser, the spectral changes shown in Figure 1 were largely abolished, and the ratio of the bands was nearly independent of laser power, as shown in Figure 2. We attribute these effects to a laser-induced photostationary state in which the ligation equilibrium is shifted toward 4-coordination; evidently the movement of the sample through the laser beam in the spinning cell (3000 rpm) is sufficient to abolish this effect.

The solid line in Figure 2 represents the equation

$$\frac{I_4}{I_6} = \frac{j_4(k_6 + I_0\sigma_6\phi_6)}{j_6(k_4 + I_0\sigma_4\phi_4)}$$

Where I_i, j_i, and σ_i are the observed Raman intensity, the molar scattering factor, and the molar absorptivity of NiTPP ($i = 4$) and $(py)_2$NiTPP ($i = 6$), ϕ_4 and ϕ_6 are the quantum yields for converting $4 \rightarrow 6$ or $6 \rightarrow 4$ via light absorption, k_4 and k_6 are the thermal interconversion rates, and I_0 is the incident laser flux. This equation derives from a simple photokinetic scheme in which photoexcited NiTPP and $(py)_2$NiTPP are interconverted via capture or loss of ligands or else return to their own ground state. From the limiting values of I_4/I_6 one can calculate $k_6\sigma_4\phi_4/k_4\sigma_6\phi_6 = 1.6/0.54 = 3.0$. From the optical absorption spectra (and the assumption that the $(py)_2$NiTPP spectrum is given by that of NiTPP in piperidine, for which $(pip)_2$NiTPP predominates) one can estimate $\sigma_4/\sigma_6 \simeq 90$ (at 406.7 nm) and k_4/k_6 (the (4)/(6) equilibrium ratio) $\simeq 1.5$, whence $\phi_4/\phi_6 \simeq 0.05$. A low ratio of quantum yields is reasonable since ligation of the photoexcited NiTPP is a bimolecular process, while ligand loss from photoexcited $(py)_2$NiTPP is unimolecular.

Figure 3 shows laser-induced changes in RR spectra of NiTPP in piperidine; again these changes are abolished by spinning the sample. The major species is the 6-coordinate complex, with $\nu_4 = 1346$ cm^{-1}. Another band is seen at 1356 cm^{-1}, which increases with increasing laser power. In addition a band grows in at 1369 cm^{-1}, the frequency of the 4-coordinate species. Thus photopumping of the deligation process is seen in piperidine as well as pyridine. The new species responsible for the 1356-cm^{-1} band is suggested to be a 5-coordinate complex, with a single piperidine ligand. The 13-cm^{-1} ν_4 decrease between the 4- and 5-coordinate species suggests an appreciable core-size expansion consistent with high-spin character for the latter, as predicted by Ake and Gouterman;[6] adding an axial ligand to NiTPP without a change in spin state would not be expected to change the core size very much. The 10-cm^{-1} increase in ν_4 of the 5-coordinate species relative to that of the 6-coordinate $(pip)_2$NiTPP (which is also high spin) may reflect partial relaxation of the core size, due to the out-of-plane displacement of the Ni atom expected for a 5-coordinate high-spin adduct, by analogy with the relaxation seen for (2-MeImH)FeTPP (2.045 Å C_t–N; Fe 0.5 Å out of plane)[16] relative to high-spin $(THF)_2$FeTPP (2.057 Å C_t–N, Fe in plane.[17] If changes in the (pip)NiTPP concentration resulted simply from adjustments of the thermal equilibrium the growth of the 1356-cm^{-1} peak would be expected to track that of the 1369-cm^{-1} peak, but the former appears to saturate with increasing laser power while the latter does not. This behavior suggests that (pip)NiTPP forms directly by photopumping $(pip)_2$NiTPP and loss of a single ligand. If the (pip)NiTPP ground state is high spin, then electronic deexcitation must be competitive with loss of a second ligand from the low-spin primary photoproduct.

Acknowledgment. This work was supported by Grant DE-ACD2-81ER10861 from the Department of Energy. We thank Professor Dewey Holten for helpful discussions.

(16) Hoard, J. L.; Scheidt, W. R. *Proc. Natl. Acad. Sci. U.S.A.* **1973**, *70*, 3913; **1974**, *71*, 1578.
(17) Reed, C. A.; Mashiko, T.; Scheidt, W. R.; Spartalian, K.; Lang, G. *J. Am. Chem. Soc.* **1980**, *102*, 2302.

Rapid Precipitation of Low Vapor Pressure Solids from Supercritical Fluid Solutions: The Formation of Thin Films and Powders

Robert C. Petersen, Dean W. Matson, and Richard D. Smith*

Chemical Methods and Separations Group
Chemical Technology Department
Battelle, Pacific Northwest Laboratories
Richland, Washington 99352

Received September 30, 1985

Supercritical fluids have been shown to have excellent solvating properties above their critical densities, and supercritical fluid solutions of solutes having negligible vapor pressures can be readily prepared.[1-5] We are currently investigating the rapid expansion of supercritical fluid solutions (RESS) to better understand the process and to evaluate the range of solute products that can be produced by the rapid loss of solvating power which occurs during expansion. Products include films, fine powders having narrow size distributions, and amorphous mixtures produced under the nonequilibrium conditions inherent in the expansion process.

* Author to whom correspondence should be addressed.

(1) Smith, R. D.; Udseth, H. R. *Anal. Chem.* **1983**, *55*, 2266-2272.
(2) Randall, L. G. *Chemical Engineering at Supercritical Fluid Conditions*; Paulaitis, M. E., Penninger, J. M. L., Gray, R. D., Davidson, P., Eds.; Ann Arbor Science: Ann Arbor, MI, **1983**; pp 477-498.
(3) Hannay, J. B.; Hogarth, J. *Proc. R. Soc. London* **1879**, *29*, 324-326.
(4) Hannay, J. B.; Hogarth, J. *Proc. Roy. Soc. London* **1880**, *30*, 178-188.
(5) Paulaitis, M. E.; Krukonis, V. J.; Kurknik, R. T.; Reid, R. C. *Rev. Chem. Eng.* **1983**, *1*, 179-250.
(6) Anderson, J. B. *Molecular Beams and Low Density Gas Dynamics*; Wegener, P., Ed.; Marcel Dekker: New York, 1971.
(7) Shapiro, A. H. *Compressible Fluid Flow*; Ronald Press: New York, 1953; Vol. I, pp 159-186.
(8) Murphy, H. R.; Miller, D. R. *J. Phys. Chem.* **1984**, *88*, 4474-4478.

0002-7863/86/1508-2100$01.50/0

Table I. Typical Experimental Parameters and Product Morphogies of RESS-Deposited Materials[a]

solute–solvent	autoclave temp., °C	system press., bar	preexpansion temp., °C	product morphology
SiO_2–H_2O	260	580	450	>1.0-μm-thick film (Figure 1a)
SiO_2–H_2O	300	590	470	0.1–0.5-μm-diameter spheres (Figure 1b)
GeO_2–H_2O	25	580	475	5-μm agglomerates (Figure 1c)
GeO_2–H_2O	25	580	445	0.5–1.3-μm-diameter spheres (Figure 1d)
SiO_2, KI–H_2O	385	580	500	20-μm agglomerates[b]
Si–NH_3	250	284–415	350	no product[c]
SiO_2–NH_3	285	204	350	no product[c]
Si_3N_4–NH_3	160–385	136–306	280–410	no product[c]
polystyrene–pentane	200	170	350	20-μm-diameter spheres[d]
polystyrene–pentane	200	170	200	1-μm-diameter fibers of 100–1000-μm length[d]
polypropylene–pentane	225	170	200–400	1-μm-diameter fibers of 100–1000-μm length or 0.5–1.0-μm particles[e]
polycarbosilane–pentane	*f*	102	375	1-μm-diameter fibers of 20–160-μm length
polycarbosilane–pentane	*f*	238	250	<0.1-μm particles
polyphenyl sulfone–propane	125	170	150	agglomerated spheres (each sphere 0.5-μm diameter)
polymethyl methacrylate–propane	125	170	125–300	1-μm-diameter fibers of 100–1000-μm length of 0.5–1.0-μm particles[e]
polyvinyl chloride, KI–Ethanol	250	170	350	7-μm-diameter spheres[g]

[a] All expansion nozzles were 5 mm in length. Systems containing organic solvents used a 25-μm-i.d. fused silica capillary nozzle. Inorganic solvents used a 60-μm-i.d. stainless steel capillary. [b] X-ray fluorescence indicated the presence of both products in each agglomerate. [c] Solubility was too low to detect any RESS product. [d] The 300 000 molecular weight polystyrene used, had a melting point of ≈170 °C. Fibers were formed with the preexpansion temperature near the melting point, otherwise spherical particles were produced. [e] As with polystyrene, the preexpansion temperature determined product morphology (see note *d*). [f] No autoclave was used. Instead a 3230 ppm (by weight) solution preheated to 375 °C before expansion produced fibers. A 34.8 ppm solution preheated to 250 °C produced particles. [g] X-ray fluorescence indicated the presence of both products in spherical particles.

The RESS process typically involves dissolving a solid in a solvent at an elevated temperature and pressure where the solubility is considerably enhanced. The resulting solution is heated to supercritical conditions in a preexpansion region and subsequently allowed to expand rapidly through a short nozzle (typically 5 mm long and 25- or 60-μm i.d. in this work) into a low-temperature and -pressure environment where the fluid solvating power is negligible. The time scale of the RESS process is in the 10^{-8}–10^{-5} s range. This encourages the rapid nucleation and growth of solute particles, provided sufficient solute density exists in the expansion jet. Significant cooling occurs in the expanding jet, resulting from the isentropic phase of the decompression and the generally positive Joule–Thomson expansion coefficient for the range of relevant conditions.[6-8] However, under proper preexpansion conditions (generally reduced temperatures above 1.3), sufficient thermal energy remains to suppress fluid droplet formation during the expansion and the product is collected under essentially "dry" conditions. At lower fluid temperatures a two-phase gas/liquid region is traversed during the expansion, producing droplets. This has been experimentally confirmed by the visual observation of the RESS jet through a wide range of temperatures and pressures.

The morphology of deposition products was examined utilizing optical microscopy or scanning electron microscopy. Qualitative X-ray fluorescence was applied for elemental analysis of particles in representative samples and when multicomponent products were expected. The amorphous nature of RESS-produced silica powders was confirmed by powder X-ray diffraction, and surface areas were measured by nitrogen gas adsorbtion (BET method) to be 13.7 m^2/g for a typical sample. The absence of solvent in 100 000 molecular weight polystyrene products precipitated from supercritical pentane–ethanol mixtures was confirmed by Fourier transform infrared analysis. The melting point of a polypropylene product was <10 °C lower than that of the starting material, indicating very little fractionation by selective solvation of the lower molecular weight oligomers under selected operating conditions.

Table I summarizes some of our initial observations concerning RESS materials and product morphologies for typical deposition conditions. Examples of several RESS products are shown in Figure 1. Uniform films or coatings can be deposited by the RESS process, as shown in Figure 1a, in which a relatively thick film (>1.0 μm) of amorphous silica has been deposited on a Millipore filter. The surface of this film has cracked due to flexing of the substrate, demonstrating the continuous nature of the surface. Under different experimental conditions, silica may also form discreet particles with a relatively narrow size distribution, as shown in Figure 1b. Solute concentration, controlled by manipulating temperature in the dissolution region, has been demonstrated to greatly affect particle size. Silica particles ranging from <0.01- to 0.5-μm diameter were obtained by expansion of silica solutions over an estimated concentration range of <10 to 500 ppm.

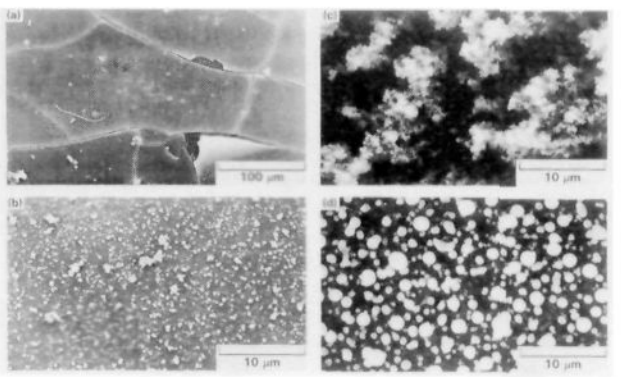

Figure 1. Examples of products from rapid expansion of supercritical water solutions: (a) Film of amorphous SiO_2 (>1.0 μm thick) deposited on a Millipore filter at 450 °C and 580 bar with expansion region pressure of 0.1 bar. (b) SiO_2 particles deposited at 470 °C and 590 bar with expansion region pressure of 0.1 bar. (c,d) GeO_2 particles deposited under identical conditions (580 bar of fluid pressure and 1-bar expansion-region pressure) except for preexpansion temperatures of 475 °C (c) and 445 °C (d). In all cases, the expansion nozzle was 60-μm-i.d. stainless steel.

Figure 1c,d illustrates another effect on deposition characteristics which can be produced by relatively minor variations in preexpansion temperature. Figure 1c shows a highly agglomerated and porous mass of very small GeO_2 particles deposited by expansion of supercritical water at 475 °C. Figure 1d shows spherical particles collected at 445 °C (only 30 °C lower than Figure 1c). We hypothesize that this change in morphology reflects the greater importance of intermediate solvent cluster or droplet formation at the lower temperature.

Precipitation of low vapor pressure solids from rapid expansion of a supercritical fluid solution allows formation of amorphous, finely divided powders and thin films from organic and inorganic materials. Our work has demonstrated the ability to control the particle size, at least over limited ranges (e.g., between 0.01 and

0.5 μm for silica). Future studies will be aimed at more detailed product characterization and quantization of experimental parameters controlling particle formation and generation of intimate mixtures of substances by this nonequilibrium process.

Acknowledgment. The support of Battelle, Pacific Northwest Laboratories, and Battelle Memorial Institute through Corporate Technical Development Project 2322247110/B-03330-4250 is acknowledged.

Lithium–Metalloid Exchange Reactions.[1] Observation of Lithium Pentaalkyl(aryl) Tin Ate Complexes

Hans J. Reich* and Nancy H. Phillips

McElvain Laboratories of Organic Chemistry
Department of Chemistry, University of Wisconsin
Madison, Wisconsin 53706

Received December 9, 1985

The lithium–tin exchange reaction has become one of the premier methods for the preparation of vinyl-, aryl-, and even alkyllithium reagents in situations where other less expensive methods such as the reduction of halides or metalation are not selective or mild enough to be effective.[2,3] Although some kinetic work has been done,[4] the mechanism of this interesting transformation has not been established securely but has generally been assumed to proceed through a four-centered transition state. An alternative mechanism involving intermediate "ate" complexes has been proposed.[3] We have experimentally addressed the question of whether such previously undetected intermediates may actually be present in finite concentrations and offer here convincing spectroscopic evidence that this is the case.

Figure 1 shows a series of ^{119}Sn NMR spectra of THF solutions containing methyllithium and tetramethyltin (3:2) to which increasing amounts of HMPA were added. In pure THF only the tetramethyltin signal at 0 ppm was visible. As the concentration of HMPA was increased, a new signal at −277 ppm appeared[5] and grew at the expense of the tetramethyltin peak until that signal disappeared entirely. Careful analysis of the ^1H-coupled multiplet of both the normal and INEPT[6] spectra revealed that the best match between experimental and calculated line intensities occurs for a tin split equally by 15 protons.

Solutions of tetramethyltin and methyllithium in THF/HMPA show dynamic NMR behavior in the ^1H, ^{13}C, and ^{119}Sn spectra at temperatures between −80 and −20 °C. For example, the 270-MHz ^1H spectra of a solution 0.3 M CH_3Li, 0.16 M in $(CH_3)_4Sn$, and 0.4 M in HMPA showed broadening and partial coalescence of the signals assigned to CH_3Li, $(CH_3)_4Sn$, and a third species which we have identified on the basis of this and other spectroscopic evidence (Table I) as $Li^+Sn(CH_3)_5^-$. Although decomposition (formation of methane) and dramatic temperature dependence of the equilibrium constant complicate proper kinetic analysis of the spectra, they do serve to demonstrate that the three species are interconverted by an exchange process.

Solutions of mixed phenyl methyl complexes (**1**) were analogously prepared by the careful low temperature (<−80 °C) addition of the organostannane to methyl- or phenyllithium in

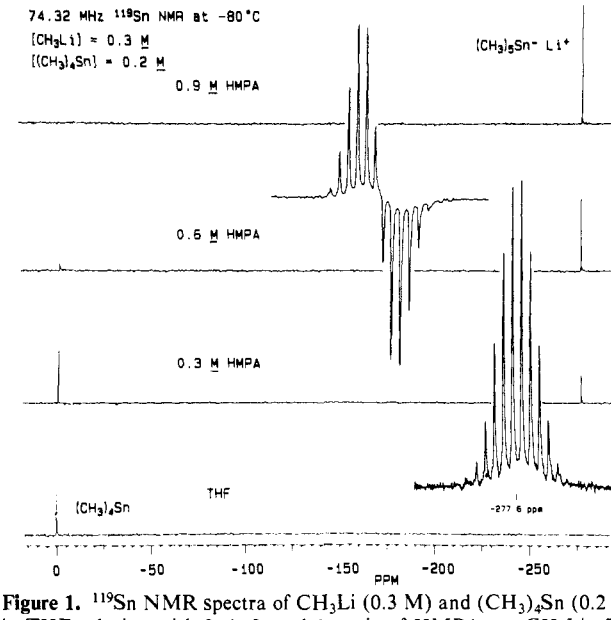

Figure 1. ^{119}Sn NMR spectra of CH_3Li (0.3 M) and $(CH_3)_4Sn$ (0.2 M) in THF solution with 0, 1, 2, and 3 equiv of HMPA per CH_3Li. The inset shows ^1H coupled expansions of the signal at −277 ppm using a normal and an INEPT[6] pulse sequence. Peak separation is 39 Hz.

Table I. Observed (Calculated) ^{13}C and ^{119}Sn Parameters for $Me_{5-m}Ph_mSn^-Li^+$ at −80 °C

● = C_6H_5 ○ = CH_3

Parameter:	δ_{Sn}	δ_C (Me)	$^1J_{Sn-Me}$	δ_C (Ph)[b]	$^1J_{Sn-Ph}$
Apical:[a]			(−17 Hz)	(180 ppm)	(80 Hz)
Equat:[a]			(441 Hz)	(151 ppm)	(640 Hz)
$(CH_3O)_3Sn^-$	−277	6.3	257 (258)	-	-
$(CH_3O)_2(C_6H_5)Sn^-$	−291	3.3	375 (327)	182.2 (180)	80 (80)
$(CH_3O)(C_6H_5)_2Sn^-$	−311	−1.0	450 (441)	180.0 (180)	60 (80)
$(CH_3O)_3Sn^-$	−300	−2.3	450 (441)	170.6 (170)	250 (267)
$(CH_3O)_2(C_6H_5)Sn^-$	−292	−2.3	436 (441)	165.0 (163)	376 (360)
$(C_6H_5)_3Sn^-$	−303	-	-	161.9 (161)	427 (416)

[a] Parameters in parentheses were calculated by using the optimum axial and equatorial values listed at the top of each column. [b] C-1 of phenyl.

(1) For previous papers in this series, see: (a) Reich, H. J.; Phillips, N. H.; Reich, I. L. *J. Am. Chem. Soc.* **1985**, *107*, 4101. (b) Reich, H. J.; Yelm, K. E.; Reich, I. L. *J. Org. Chem.* **1984**, *49*, 3438. (c) Reich, H. J.; Chow, F.; Shah, S. K. *J. Am. Chem. Soc.* **1979**, *101*, 6638.

(2) (a) Seyferth, D.; Weiner, M. A.; Vaughan, L. G.; Raab, G.; Welch, D. E.; Cohen, H. M.; Alleston, D. L. *Bull. Soc. Chim. Fr.* **1963**, 1364. (b) Piers, E.; Karunaratne, V. *J. Org. Chem.* **1983**, *48*, 1774. Goswami, R. *J. Am. Chem. Soc.* **1980**, *102*, 5973. Seyferth, D.; Murphy, G. J.; Mauze, B. *J. Am. Chem. Soc.* **1977**, *99*, 5317. Seyferth, D.; Wursthorn, K. R. *J. Organomet. Chem.* **1977**, *137*, C17. Corey, E. J.; Eckrich, T. M. *Tetrahedron Lett.* **1984**, *25*, 2415; Peterson, D. J. *J. Am. Chem. Soc.* **1971**, *93*, 4027. Quintard, J. P.; Elissondo, B.; Pereyre, M. *J. Org. Chem.* **1983**, *48*, 1559.

(3) (a) Meyer, N.; Seebach, D. *Chem. Ber.* **1980**, *113*, 1290. (b) Sawyer, J. S.; Macdonald, T. L.; McGarvey, G. J. *J. Am. Chem. Soc.* **1984**, *106*, 3376. (c) Still, W. C.; Sreekumar, C. *J. Am. Chem. Soc.* **1980**, *102*, 1201. Still, W. C. *J. Am. Chem. Soc.* **1978**, *100*, 1481. (d) Wittig, G.; Schollkopf, U. *Tetrahedron* **1958**, *3*, 91. (e) Kauffmann, T.; Kriegesmann, R.; Altepeter, B.; Steinseifer, F. *Chem. Ber.* **1982**, *115*, 1810.

(4) Batalov, A. P.; Podogina, L. A. *Khim. Elementoorg. Soedin.* **1978**, *6*, 46; *Chem. Abstr.* **1980**, *92*, 40915.

(5) (a) High-field ^{119}Sn chemical shifts are characteristic of penta- and hexacoordinated tin compounds: Weichmann, H.; Mugge, C.; Grand, A.; Robert, J. B. *J. Organomet. Chem.* **1982**, *238*, 343. Davies, A. G.; Harrison, P. G.; Kennedy, J. D.; Mitchell, T. N.; Puddephat, R. J.; McFarlane, W. *J. Chem. Soc. C* **1969**, 1136. (b) Petrosyan, V. S. *Progr. NMR Spectrosc.* **1977**, *11*, 115. (c) Nadvornik, M.; Holecek, J.; Handlir, K.; Lycka, A. *J. Organomet. Chem.* **1984**, *275*, 43.

(6) Doddrell, D. M.; Pegg, D. T.; Bendall, M. R. *J. Magn. Reson.* **1982**, *48*, 323; Doddrell, D. M.; Pegg, D. T.; Brooks, W.; Bendall, M. R. *J. Am. Chem. Soc.* **1981**, *103*, 727.

0002-7863/86/1508-2102$01.50/0